CHINESE OPTICS LETTERS

Vol. 19, No. 5 | May 2021

Topological photonic states in artificial microstructures [Invited]

Hui Liu (刘 慧)[1], Boyang Xie (谢博阳)[1], Hua Cheng (程 化)[1*], Jianguo Tian (田建国)[1], and Shuqi Chen (陈树琪)[1,2,3**]

[1] Key Laboratory of Weak Light Nonlinear Photonics, Ministry of Education, School of Physics and TEDA Institute of Applied Physics, Nankai University, Tianjin 300071, China

[2] Collaborative Innovation Center of Extreme Optics, Shanxi University, Taiyuan 030006, China

[3] Collaborative Innovation Center of Light Manipulations and Applications, Shandong Normal University, Jinan 250358, China

*Corresponding author: hcheng@nankai.edu.cn

**Corresponding author: schen@nankai.edu.cn

Received October 24, 2020 | Accepted December 21, 2020 | Posted Online January 19, 2021

Topological photonics provides a new opportunity for the examination of novel topological properties of matter, in which the energy band theory and ideas in topology are utilized to manipulate the propagation of photons. Since the discovery of topological insulators in condensed matter, researchers have studied similar topological effects in photonics. Topological photonics can lead to materials that support the robust unidirectional propagation of light without back reflections. This ideal transport property is unprecedented in traditional optics and may lead to radical changes in integrated optical devices. In this review, we present the exciting developments of topological photonics and focus on several prominent milestones of topological phases in photonics, such as topological insulators, topological semimetals, and higher-order topological phases. We conclude with the prospect of novel topological effects and their applications in topological photonics.

Keywords: topological photonics; states; artificial microstructures.

DOI: 10.3788/COL202119.052602

1. Introduction

In the last two decades, artificial microstructures including metamaterials and photonic crystals have attracted enormous interest because they provide great possibilities for manipulating optical waves. By judiciously modulating their structural parameters, the effective values of the permeability and permittivity can be designed deliberately to realize novel functionalities beyond the capability of natural materials[1–3]. Metamaterials are three-dimensional (3D) artificial nanostructures, which can be designed to manipulate optical waves in a specific dimension with desirable optical functionalities, such as negative refractive index[1], invisibility cloaks[3], and chiral media[4]. Metasurfaces as planar metamaterials have paved the way to arbitrarily manipulate the amplitude, polarization, phase, and frequency of optical waves in an effective way[5–8]. They can be widely applied in polarization conversion[9], beam deflectors[10], optical sensors[11], metalenses[12], structural colors[13], and nonlinear optics[14,15]. Photonic crystals as periodically arranged optical nanostructures with photonic band structures have become a key platform for studying optical phenomena in periodic structures. The controlling and manipulating of light in photonic crystals is based on the modulation of periodic potential, which is similar to electronic systems[16,17]. The approach to control light in periodic systems exploits photonic band structures that stem from Bragg scattering or localized resonance[18]. The photonic band structure can be designed and tuned conveniently, giving rise to potential applications in subwavelength imaging[19,20], wave transportation[21], and mimicking quantum effects[22]. Topology that characterizes the quantized global behavior of the wavefunctions on the entire band structure has aroused great interest in photonics[23].

The idea of topological physics originated from the exciting discovery of the integer quantum Hall effect (IQHE) in condensed-state physics. Klitzing found that two-dimensional (2D) electron gas in a strong perpendicular magnetic field has a quantized Hall conductance[24]. The quantization originates from the nontrivial topology of the energy band structure, which is characterized by the Chern number according to the theoretical work of Thouless, Kohmoto, Nightingale, and den Nijs (TKNN)[25]. Haldane and Raghu creatively introduced the concept of topology to photonic crystals for the first time, to the best of our knowledge, as they proposed a photonics analogue of the quantum Hall effect in photonic crystals[26,27]. Edge states

© 2021 Chinese Optics Letters

appear at the domain wall between materials that have different Chern numbers and go through the topological bandgap in momentum space according to the bulk-edge correspondence[28–30]. As the topological invariants of the system cannot change under perturbations or deformations unless the band gap is closed somewhere, the edge states are immune to defects and backscattering, resulting in the robust transportation of the edge states. Such time-reversal (T)-symmetry breaking topological gapped phases have proven useful in the design of novel optical devices[31–36]. Related design concepts of topological physics are also realized in other periodic systems such as phononic crystals[37,38], ultracold atomic gases[23,39,40], and classical mechanical systems[41–43].

Previous studies of IQHE in photonics systems depended on the magneto-optical effect in gyromagnetic materials at microwave frequencies, which limits the application of topological edge states in the optical domain. The discovery of quantum spin Hall effect (QSHE) in HgTe quantum wells[44–47] showed another way to achieve topological states without applying magnetic fields. Several schemes for QSHE have been proposed in various photonic systems, such as coupled resonator optical waveguides[48,49], bianisotropic metamaterials[50,51], and point group symmetry-protected photonic crystals[52,53], which have greatly promoted the development of topological photonics. To construct a Kramers-like degeneracy, pseudospin degrees of freedom are introduced in photonic systems, where each pseudospin meets an artificial magnetic field with the protection of pseudo-T symmetry. Protected by T symmetry, the Chern number is zero, but the Z_2 topological invariant is nonzero in the system. A pair of topological edge states with opposite propagation directions was observed in the topological band gaps. This phenomenon has several possible revolutionary applications in edge or surface optics.

Many studies have exploited the advantages in bosonic systems, including photonic and acoustic systems[54–59]. For example, the study of the photonic topological phase has also been extended to 3D photonic semimetals, where the topological charge can be featured by the Chern number and Z_2 topological invariant[60]. The entire spectrum of topological materials can be exploited because the Fermi levels are substituted with frequency in photonic systems, which means the equi-frequency contour of bulk and surface states in topological semimetals can be tuned by the frequency. The easier fabrication also allows the delicate design of the interface, edge, and corner, which greatly facilitates the study of higher-order topological states. In addition, time-dependent periodic modulation can be added to the structural design, resulting in Floquet topological insulators (TIs)[61–64] and topological pumping[65–67]. Moreover, photonics systems have great advantages in the research of topological non-Hermitian photonic crystals[68–70]. The non-Hermiticity is introduced in the effective Hamiltonians when the gain and loss of optical materials are considered. Topological invariants such as the non-Hermitian Chern number and the vorticity of the energy eigenvalues are defined in non-Hermitian systems. In particular, parity-time (PT) symmetry can be established with balanced gain and loss profiles. PT synthetic photonic lattices have been experimentally realized using coupled fiber loops[71], microcavities[72], and metamaterials, which can be applied in many fields, such as unidirectional invisibility or reflection[71], coherent perfect absorption[73,74], light–light switching[75], and lasing[72,76]. Nonlinear optical media can also give rise to exotic phenomena such as solitons supported in a photonic TI[77,78], self-induced topological transitions[79,80], and strongly correlated photon states[81–83]. In addition, a new topological phase of atomic matter, known as Skyrmions, was realized in optical Skyrmion lattices very recently[84,85].

In this review, we introduce two types of topological gapped phases, IQHE and QSHE, and their realization in photonic crystals, coupled wave guides, and metamaterials. Then, we extend the discussion to topological gapless phases, such as 3D photonic semimetals, where the Weyl points, 3D Dirac points, and nodal structure and their surface states are discussed. In the last section, we introduce the recent progress in higher-order phases that rise beyond the conventional bulk–boundary correspondence.

2. Photonic Integer Quantum Hall Effect

With the discovery of the topological phases of matter in solid-state materials, researchers began to explore topological properties in photonic crystals. Inspired by the study of 2D electron gas in electronic materials, the scheme of the 2D photonic IQHE was proposed for the first time, to the best of our knowledge, by Haldane and Raghu based on the Dirac equation[26]. For a hexagonal-lattice photonic crystal protected by T symmetry and parity inversion (P) symmetry, Dirac points with linear dispersion relation could appear at highly symmetric points in reciprocal space. The massless quasiparticle properties near the Dirac points can be described by the effective Hamiltonian,

$$H(\mathbf{k}) = v_x k_x \sigma_x + v_y k_y \sigma_y, \tag{1}$$

where v_i are the group velocities, k_i are the basis vectors in reciprocal space, and σ_i are the Pauli matrices. A perpendicular magnetic field is applied to break the T symmetry and then open the topological band gap. An additional mass term $\Delta_m \sigma_z$ arises in the Hamiltonian as T symmetry is broken. The bulk bands in this system carry nonzero Berry curvature, and its topological invariant is described by the first Chern number[25]:

$$C = \frac{1}{2\pi} \oiint \mathcal{F}(\mathbf{k}) \cdot \mathrm{d}\mathbf{s}, \tag{2}$$

where $\mathcal{F}(\mathbf{k}) = \nabla_k \times \mathcal{A}(\mathbf{k})$ is the Berry curvature, and $A(\mathbf{k}) = \langle u(\mathbf{k}) | i\nabla_k | u(\mathbf{k}) \rangle$ is the Berry connection.

Wang *et al.* pointed out that Dirac points are not necessary for 2D photonic IQHE. A more specific and universal scheme was proposed in a square-lattice crystal operating at microwave frequencies[86]. By using a photonic crystal consisting of a gyromagnetic ferrite rod, they realized 2D photonic IQHE at microwave frequencies for the first time[87], to the best of our knowledge. The experiment is based on a 2D waveguide, as

shown in Fig. 1(a), where an interface is set between the rods and metal walls. When a uniform magnetic field is applied to break the T symmetry, unidirectional backscattering-immune states occur in a topological band gap. The simulated field of unidirectional topological states is shown in Fig. 1(b), which propagates around arbitrary obstacles. Moreover, if the bandgap is achieved by simultaneously gapping multiple degeneracies, the application of an external magnetic field will lead to a larger gap Chern number, and the appearance of multiple unidirectional topological edge modes in the band gap. Skirlo *et al.* realized large gap Chern numbers at higher frequency bands in a 2D ferrimagnetic photonic crystal, where the gap Chern number would vary with the strength of the applied magnetic field[88,89].

The 3D photonic IQHE has also been proposed, which can be viewed as an extension of the 2D case. The corresponding topological invariant of the system can be described by the first Chern numbers in three directions: $\mathbf{C}_1 = (C_1^x + C_1^y + C_1^z)$. Recently, Lu *et al.* realized a 3D Chern photonic crystal by a plainly modulated magnetic double gyroid (DG) in the presence of a magnetic field[90]. The double-cell of a magnetic DG photonic crystal is designed to fold a pair of Weyl points into a 3D Dirac point in the band structure, as shown in Figs. 1(c) and 1(d). By applying an external magnetic field to plainly modulated DG, the 3D Dirac point is lifted in Figs. 1(e) and 1(f), resulting in the realization of topological band gaps.

As discussed above, the necessary condition for the generation of topological Chern insulators is T-symmetry breaking, which depends on the magnetic responses in the gyromagnetic photonic crystal. The T-symmetry breaking topological gapped phases in gyromagnetic photonic crystals have been studied extensively, and their unidirectional backscattering-immune edge states are expected to have a deep impact on new optical devices[32,91–94]. However, owing to the weak magnetic response in optical materials and the difficulty in device integration because of the external magnetic field, the use of topological Chern insulators in optical devices remains a challenge.

3. Photonic Quantum Spin Hall Effect

Photonic QSHE can be realized without breaking the T symmetry, which makes it more suitable for practical applications. In the electron system, QSHE relies on the degeneracy of conjugate pairs formed by spin-up and spin-down states under T symmetry, known as Kramers degeneracy. Each bulk band with spin-up or spin-down states can be described by a topological invariant C_+ or C_- in Eq. (2). Because of the protection of T symmetry, the Chern number $C = (C_+ + C_-)/2$ of the system is zero, and the topological properties of the system can be described by the spin Chern number instead of the Chern number. The spin Chern number in the system can be defined as $C_s = (C_+ - C_-)/2$, analogous to the case of an electronic Z_2 TI. The key difference between electrons and photons is that the former is a spin-1/2 fermion, while the latter is the spin-1

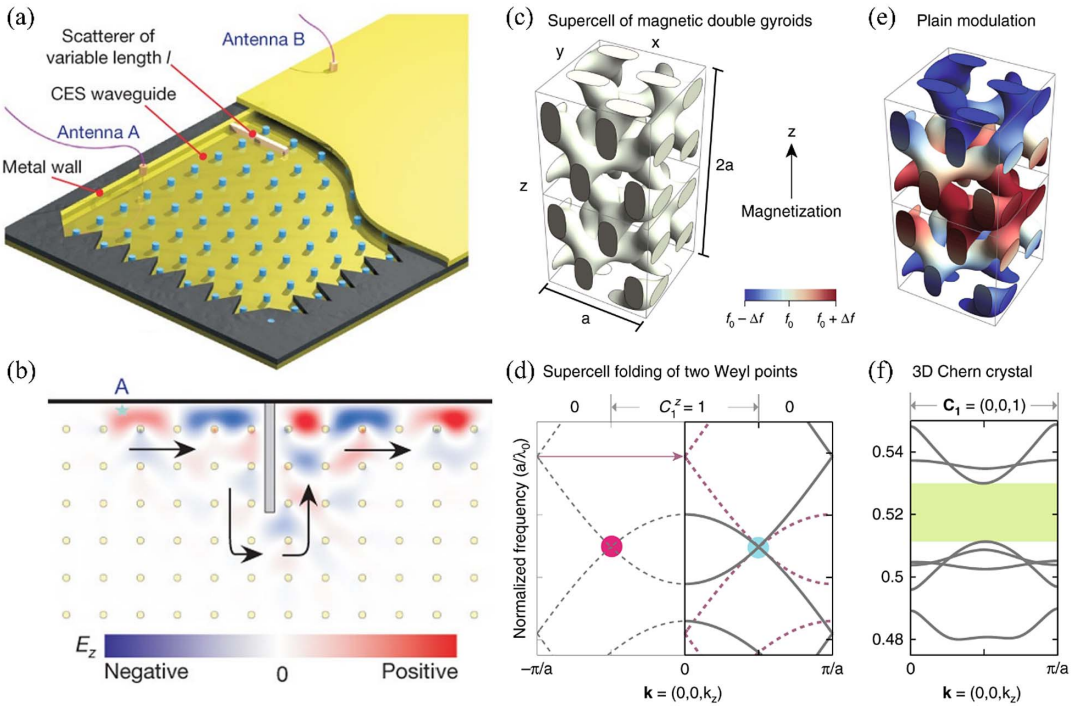

Fig. 1. (a) Experimental setup for a 2D waveguide with gyromagnetic photonic crystal geometry and metal walls. (b) Simulated propagation of chiral edge states around obstacles on the application of a uniform magnetic field. (c) Supercell of the DG photonic crystal magnetized along *z*. (d) The band structure of 3D Dirac point (blue) folding of two Weyl points (red) in the supercell. (e) The modulation of the supercell period in the *z* direction. (f) The band structure of the 3D Chern crystal.

boson, which lacks intrinsic twofold degeneracy in the spin degree of freedom. According to Kramers theorem, the QSHE requires that the fermionic T operator $\mathcal{T}$ follows $\mathcal{T}^2 = -1$, while the bosonic T operator $\mathcal{T}$ follows $\mathcal{T}^2 = +1$. In order to eliminate the influence of bosons and realize QSHE, pseudospin degrees of freedom and pseudo-T symmetry $\mathcal{T}^2 = -1$ were introduced into the photonic system to construct Kramers-like degeneracy. For spinless cases lacking Kramers degeneracy, such as photonics, acoustics, and mechanics, a pair of conjugate states corresponding to pseudospin-up and pseudospin-down can be constructed. Degeneracy similar to Kramers' degeneracy can exist under the protection of certain artificial gauge symmetries.

Several schemes have been introduced for realizing the photonic QSHE. Khanikaev *et al.* proposed a theoretical method by using the degrees of freedom of the TE and TM polarization of light[51]. In a metacrystal comprising a hexagonal lattice of spin-degenerate metamaterials, two pseudospin states TE + TM and TE−TM are constructed, and the Kramers-like degeneracy is closed and reopened by controlling the electromagnetic coupling, resulting in the realization of 2D photonic QSHE. The study shows that the interfaces of the metacrystals support spin-polarized unidirectional edge states, which makes it possible to obtain one-way propagation of photons without the application of an external magnetic field or the breaking of T symmetry. However, owing to the different responses of natural materials to the electric- and magnetic-field components, it is difficult to realize the strict condition in which the electric permittivity tensor should be equal to the magnetic permeability tensor in the experiment. He *et al.* constructed a pair of pseudospin states by left circular polarization (LCP) and right circular polarization (RCP) in a 2D photonic TI with a piezoelectric and piezomagnetic superlattice[52]. Figures 2(a) and 2(b) show the LCP and RCP photonic states on the Poincaré sphere and the 2D square-lattice Tellegen photonic crystal, respectively. In the system, Tellegen magneto-electric coupling was used as the photonic pseudospin-orbit interaction for LCP and RCP states, which breaks the bosonic T symmetry. Meanwhile, the LCP and RCP states give rise to an artificial fermionic pseudospin T symmetry. The Kramers-like degeneracy is open or closed at the M point of the Brillouin zone with (solid line) or without (dashed line) the pseudospin-orbit coupling effect, as shown in Fig. 2(c). With the pseudospin-orbit coupling effect, the projected band structure in Fig. 2(d) shows that a pair of one-way pseudospin-dependent edge states corresponding to the LCP (green line) and RCP (red line) still exists with the breaking of bosonic T symmetry. This finding shows that the necessary condition for the QSHE is the protection of an artificial fermionic-like pseudo-T symmetry in this system, which paves a new path to understand the mechanism of novel topological phenomena. QSHE with the pseudospin states of TE + TM and TE−TM was observed in bianisotropic photonic crystals[53].

A new scheme for 2D photonic QSHE is achieved by the lattice symmetry proposed by Wu and Hu[95]. A pair of photonic pseudospins was formed by hybridizing the degenerate Bloch modes in a 2D honeycomb photonic crystal with C_6 rotational symmetry[96]. The 2D photonic crystal is composed of six cylinders of dielectric material, as shown in Fig. 2(e). Based on the band-folding mechanism, the Dirac cones at the K and K' points in the first Brillouin zone of the graphene lattice are folded to doubly degenerate Dirac cones at the Γ point. Stretching or compressing the interstitial region among artificial atoms, the doubly degenerate Dirac cone is lifted into a trivial or nontrivial bandgap, resulting in band inversion between the p and d bands and the topological transition in the system, as shown in Fig. 2(f). A pair of topologically protected pseudospin-dependent helical edge states occurs at the interface between the nontrivial [right in Fig. 2(f)] and trivial photonic crystals [left in Fig. 2(f)]. Moreover, the idea based on lattice symmetry has also been applied to the quantum valley Hall effect[97,98]. The valley degree of freedom arises from the C_3 point group symmetry, where inequivalent valley occurs at the corners of hexagonal Brillouin zone. Valley-selective net spin flow is realized inside the bulk of the valley photonic crystal. Robust transmission and valley-dependent edge states can occur at the domain wall between two photonic crystals that have opposite valley Chern numbers. Compared with other proposals, this simple design, backed up by symmetry consideration, is easier to realize in experiments and has influenced the topological physics and related materials in a wide variety of systems, such as phonon systems[99], metasurfaces[100], and photonic quantum domains[101].

Another scheme was proposed in the coupled-ring resonator system by Hafezi *et al.*[48,49]. By controlling the light path traveling clockwise and counterclockwise along the ring resonator, a degenerate pair of clockwise and counterclockwise pseudospin states is constructed in the system. Meanwhile, the clockwise or counterclockwise roundtrip of light in lattice units gives rise to opposite effective gauge potentials. In this way, an effective magnetic field for photons is synthesized in this non-magnetic system. The scheme is realized based on a 2D silicon photonic platform, as shown in Fig. 2(g). In the experiment, the one-way topological-protected edge states are excited, as shown in Fig. 2(h). The trajectory of the edge states is clockwise or anticlockwise, depending on the frequency.

Inspired by the schemes for 2D photonic QSHE, 3D QSHE was also recently realized. Slobozhanyuk *et al.* proposed a theoretical 3D topological photonic metacrystal based on the concept of weak 3D TIs for the first time[102], to the best of our knowledge. Starting from a 3D Dirac point, the Dirac points are lifted by modulating a doubly anisotropic metamaterial, resulting in the occurrence of one-way topologically protected interface states. Yang *et al.* experimentally realized a 3D photonic TI at microwave frequencies[103]. The unit cell consists of connected split-ring resonators (SRRs) with strong magneto-electric coupling in a triangular lattice. The composite material behaves like a weak TI, which has an even number of surface Dirac cones. The experimental sample of the 3D photonic TI and the corresponding experimental setup are shown in Figs. 2(i) and 2(j), respectively. The domain wall is constructed by the down-oriented and up-oriented SRRs in the left and right sides of the domain, where topologically protected surface states

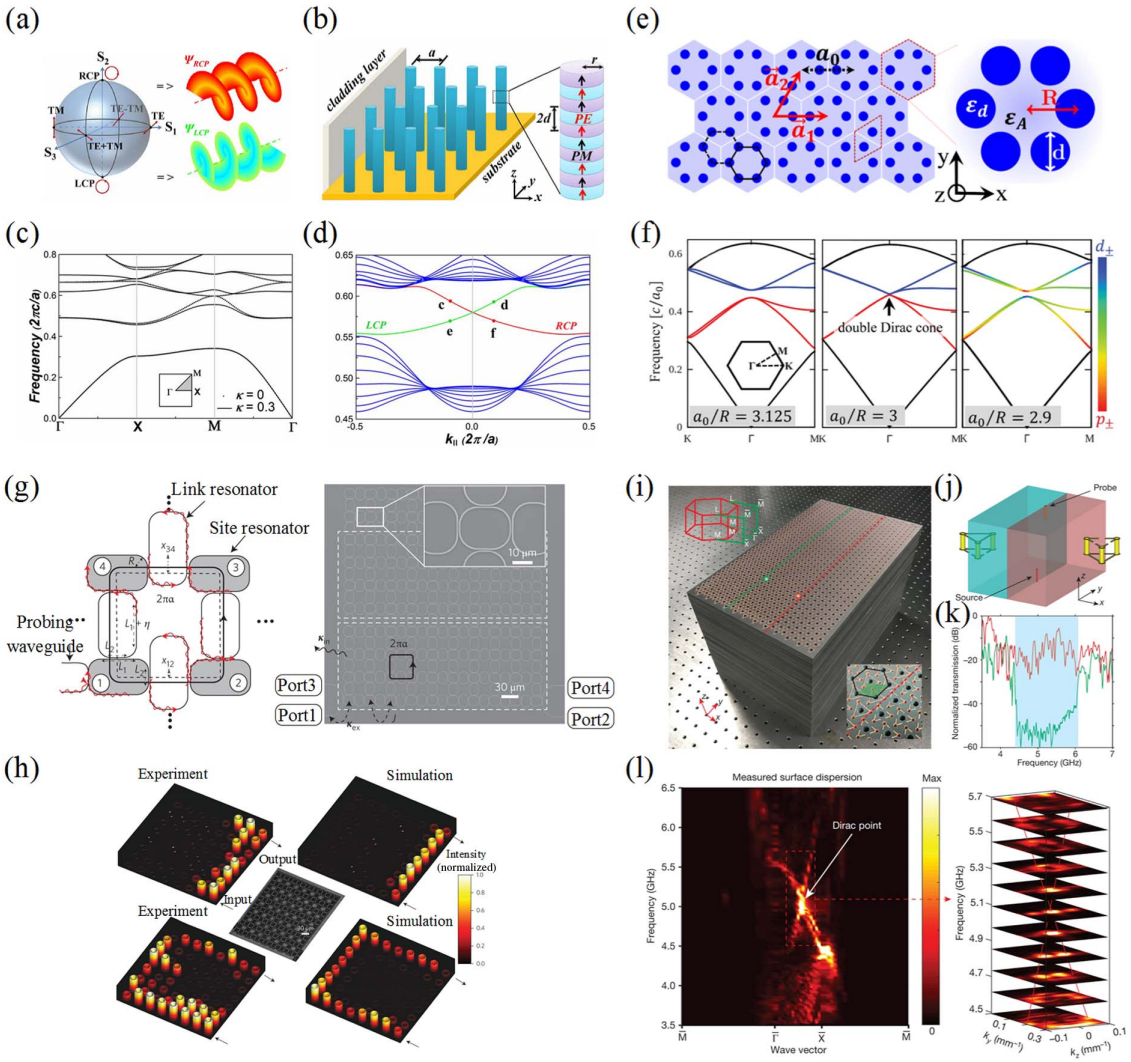

Fig. 2. (a) Polarization on the Poincaré sphere left circular polarization (LCP) (down) and right circular polarization (RCP) (up). (b) Schematic of a quasi-2D superlattice photonic crystal with alternating perfect electric/perfect magnetic layers along the z direction. (c) The band structure of the unit cell without (dotted lines) and with pseudospin coupling effect (solid lines). (d) The projected band structure whose gapless helical edge states for LCP (green line) and RCP states (red line) occur in the topological band gap. (e) Schematic of 2D dielectric photonic crystal of honeycomb lattice. (f) The band structure of the 2D photonic crystals with the lattice constant $a_0/R = 3.125$ (left), $a_0/R = 3$ (middle), and $a_0/R = 2.9$ (right). (g) Schematic of 2D silicon photonic platform with link resonators and site resonators (left) and the corresponding experimental setup diagram (right). (h) Schematic of edge states in experiment (left) and simulation (right) at different excited frequencies. (i) Schematic of 3D photonic topological insulator. (j) Experimental setup composed of two 3D photonic crystals, source, and probe. (k) Measured surface-state (red line) and bulk-state (green line) transmission. (l) Experimental observation (left) and calculated result (right) of Dirac-like topological surface states of the 3D photonic topological insulator.

exist. The transmittance (red line) remains high throughout the frequency range in Fig. 2(k), which indicates the existence of topologically protected surface states. The corresponding gapless conical Dirac-like topological surface states of the 3D photonic TI are also observed in Fig. 2(l). There is also a scheme in which the bosonic topological band structure is achieved by applying alternating magnetization to lift the 3D Dirac points discovered in the bulk of photonic crystals [104]. This 3D topological photonic crystal is a strong TI that hosts only a single surface Dirac cone.

4. Topological Semimetals

Topological semimetals have attracted much attention recently as a new type of topological gapless phase, which possess topologically protected surface states and novel topological transport phenomena[105–107]. Several types of topological semimetal band structures such as Weyl points[108], Dirac points[109], and nodal lines[110] have been successfully realized in photonic crystals.

As a 3D extension of the 2D Dirac cone, the Weyl point opens the door to the study of the 3D topological phase. Derived from

the massless solution to the Weyl Hamiltonian $H(\mathbf{k})=v_x k_x\sigma_x + v_y k_y\sigma_y + v_z k_z\sigma_z$, where v_i, k_i, and σ_i are the group velocities, momenta, and Pauli matrices, respectively, the Weyl point is the single degenerate point of two linear dispersion bands in the 3D momentum space[105,111]. Similar to magnetic monopoles, Weyl points that occur in pairs are topological monopoles of Berry flux carrying a nonzero Chern number of ±1. The surface waves, called the Fermi arc on Weyl semimetals, connect the projections of a pair of Weyl points with opposite charges on the surface and form unclosed equi-frequency dispersion curves. Lu *et al.* proposed a scheme for realizing both line nodes and Weyl points by using germanium or high-index glass in DG photonic crystals at infrared wavelengths for the first time[112], to the best of our knowledge. The Weyl points were realized by applying perturbations, breaking either T symmetry or P symmetry in the DG photonic crystals. The study showed that at least two pairs of Weyl points appear with only P-symmetry breaking, with at least one pair of Weyl points appearing with only T-symmetry breaking. The nontrivial Chern number of Weyl points can be revealed not only by the surface states, but also by the scattering matrix whose topology is equivalent to the Hamiltonian. Cheng *et al.* demonstrated a helical phase distribution in the angle (momentum)-resolved scattering matrix of electromagnetic waves in a photonic Weyl metamaterial[113]. Figure 3(b) shows the Weyl metamaterial composed of a metallic saddle-shaped connective coil. Four ideal Weyl points, whose frequencies are equal in the Brillouin zone in Fig. 3(d), hold two pairs of opposite Chern numbers distributed in the Brillouin zone, as shown in Fig. 3(c). The microwave reflection setup for the measurement of the angle-resolved reflection phase is shown in Fig. 3(e). By measuring the reflection phases for different incident azimuth angles θ, the winding phases of 2π for TE and TM eigenstates indicate that the scattering matrix carries nonzero topological invariants, as shown in Fig. 3(f). Owing to vortex reflections around the Weyl point, the Weyl metamaterial can act as a vortical mirror, where an incident Gaussian beam with spin angular momentum will be reflected with opposite spin angular momentum and an extra orbital angular momentum. The helical phase distribution further leads to spiraling Fermi arcs in an air gap sandwiched between the Weyl metamaterial and a metal plate, as shown in Fig. 3(g). The corresponding spiraling Fermi arcs at 13.3 GHz are simulated (below) and observed (above) in Fig. 3(h). The alignment-free feature of angular vortical reflection may establish a new way to manipulate optical angular momenta.

As the most basic model of topological semimetals, a series of novel topological phenomena are found in Weyl semimetals, which may provide new opportunities for unconventional control of wave propagation in photonic systems. Weyl points have also been extensively studied in many other optical systems, such as magnetized plasmas[114], photonic crystal superlattices[115], and chiral metamaterials[116,117]. In addition to the aforementioned type-I Weyl point, which has a point-like Fermi surface, there is another type of Weyl point named the type-II Weyl point, which hosts a strongly tilted dispersion and possesses a conical Fermi surface. The existence of a type-II Weyl point has been proven in various systems such as optical[118,119] and acoustic systems[58]; although it is impossible in high-energy physics because it violates the stringent Lorentz symmetry.

Hosting a fourfold linear dispersion in 3D momentum space, the 3D Dirac point represents the degeneracy of paired Weyl points with opposite chiralities. Guo *et al.* theoretically demonstrated a scheme for photonic Dirac points in a medium with homogeneous effective electromagnetic properties[120]. Recently, they observed 3D photonic Dirac points and corresponding spin-polarized surface arcs in the microwave region with a photonic metamaterial[121]. Figures 3(i) and 3(j) show the unit cell with double-layer metallic helical elements and the sample configuration for the experimental measurement, respectively. Tuning the structural parameters of the unit cell leads to two Dirac points of accidental degeneracy located on the k_z axis. The simulated band structure is shown in Fig. 3(k). The mapped band projection along the k_y direction clearly shows the existence of Dirac points experimentally, as shown in Fig. 3(l). When the source antenna excites the surface waves at the edge of the top surface at the Dirac point frequency, the Fermi arcs can be clearly observed at frequencies of 7.92 GHz, as shown in Fig. 3(m). In addition, some other types of degeneracy, such as node ring[122,123], node chain[124], and node link[125], have also been discovered in photonics.

5. Higher-Order Topological Photonic Crystals

The first-order d-dimensional topological photonic crystals have only $(d-1)$-dimensional topological edge/surface states. In contrast, higher-order d-dimensional topological photonic crystals can host topological corner states or hinge states in dimension $d-2$ or lower. The arising higher-order states go beyond the conventional bulk–boundary correspondence. In some crystalline higher-order TIs (HOTIs), the topological corner and hinge states can arise from the nontrivial bulk invariant.

The nature of higher-order topological phases has been revealed through the Berry phase framework accounting for dipole and higher electric multipole moments[126]. This theory has also been used to characterize the Bloch bands of bosonic systems such as the photonic[127] or phononic crystals[128]. The simplest realizations of 2D photonic HOTIs are based on the 2D Su–Schrieffer–Heeger (SSH) model. The emergence of corner states is rooted in the topological polarization (dipole moment), which characterizes the displacement of the average position of the Wannier center from the center of the unit cell[129]. Bulk polarization in 2D photonic crystals is defined as

$$P_i = -\frac{1}{(2\pi)^2}\int_{\mathrm{BZ}} \mathrm{d}^2\mathbf{k}\,\mathrm{Tr}[A_i], \quad i=1,2. \tag{3}$$

Here, $A_i(\mathbf{k}) = i\langle\psi_m(\mathbf{k})|\partial_{k_i}|\psi_n(\mathbf{k})\rangle$ is the Berry connection, m and n denote the eigenstates of the mth and nth bands, and i denotes the direction of reciprocal-lattice vectors.

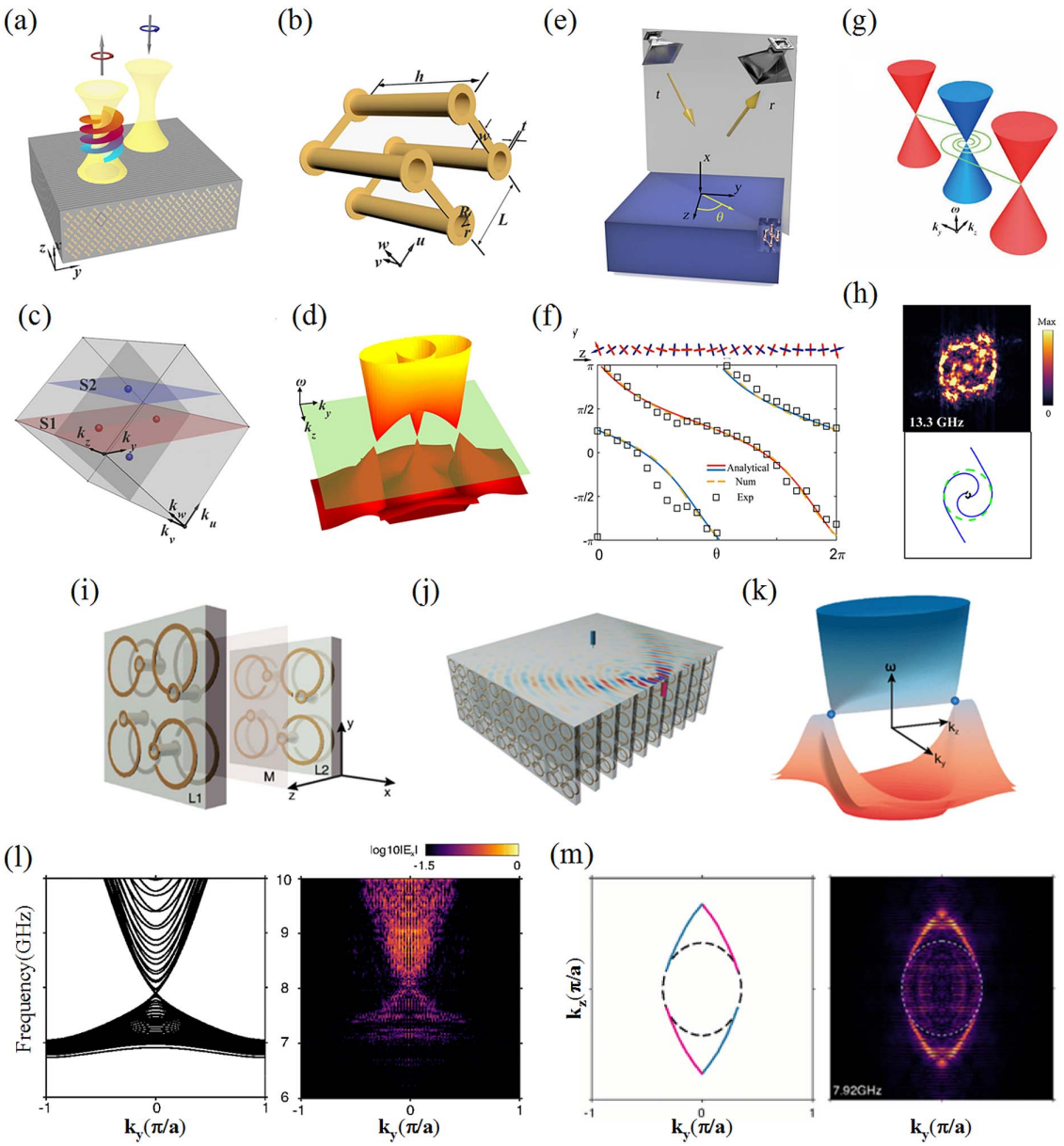

Fig. 3. (a) Schematic of the vortical mirror in Weyl metamaterial. (b) The Weyl metamaterial composed of the metallic saddle-shaped structure. (c) The distribution of ideal Weyl points in Brillouin zone. (d) The overlapped band structures of S_1 and S_2 planes showing ideal Weyl points. (e) Schematic of the reflection measurement setup in microwave. (f) Reflection phases of the Weyl metamaterial. (g) Schematic of spiraling Fermi arcs. (h) Simulation and experiment of the spiraling Fermi arc at 13.3 GHz. (i) Schematic of 3D photonic Dirac metamaterial. (j) Sample configuration for the experimental measurement. (k) The full wave simulation of 3D photonic Dirac point. (l) Experiment (right) and simulation (left) results of 3D photonic Dirac points along the k_y direction. (m) Experiment (right) and simulation (left) results of surface-state arcs at the frequency of Dirac point.

A second-order topological photonic insulator with a breathing kagome lattice is shown in Fig. 4(a)[130]. The expanded unit cell has a larger inter-cell coupling than the intra-cell coupling and a bulk polarization of (1/3, 1/3) relative to the shrunken unit cell. The non-vanishing bulk polarization shifts the Wannier center to the boundary. When the boundary separates the charge associated with the Wannier center, dangling edge/corner states emerge at the boundary. Figure 4(b) shows the energy spectrum in trivial and topological regimes, which is verified by the experimentally measured density of states in Fig. 4(c). Figure 4(d) shows the corner states at the interface between the expanded and shrunken domains. A special new class of higher-order topological corner states is found in the photonic crystal, when far-field interactions among non-neighboring unit cells are inevitable[130]. Based on the same principle, the corner states of light are also realized in photonic coupled waveguides with breathing kagome lattices[131]. In addition to the kagome lattices with C_3 symmetry, the nontrivial bulk polarization (1/2, 1/2) and corner states can also appear in the expanded C_4 symmetric lattice[132–134].

The quadrupole moment can contribute to more robust topological corner states than the nontrivial bulk polarization[127,135]. Figure 4(e) shows a 2D lattice of the nanophotonic silicon-ring resonator. The magnitude of the coupling between the lattice sites was controlled by adjusting the gap between the site-ring and the link-ring waveguides. The inter-cell coupling is stronger than the intra-cell coupling, resulting in nontrivial dipole polarization. The effective hopping phase $\varphi = \pi$ is induced by vertically shifting the link ring. This results in a net gauge flux π threading the unit cell. The system obtains a nontrivial

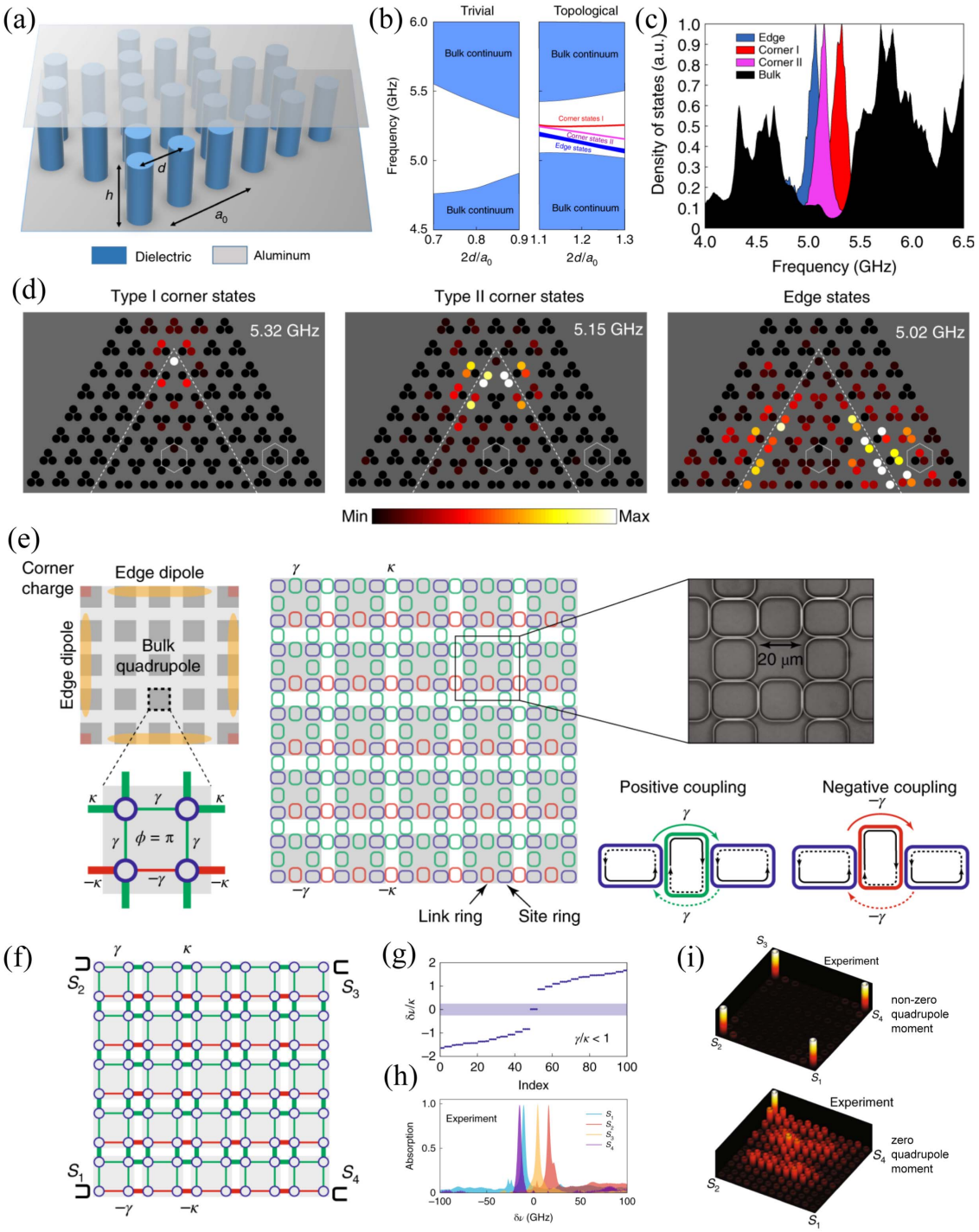

Fig. 4. (a) Schematic of the photonic crystal with kagome lattice. (b) Energy spectrum in trivial and topological regimes. (c) Experimentally measured density of states. (d) Field profile of topological corner states (type I and type II) and edge state. (e) Schematic of the photonic quadrupole topological system. (f) Schematic of the 2D lattice with quadrupole moment. The waveguide couplers are located at the four corners. (g) Energy spectrum with four degenerate corner states in the bandgap. (h) Measured power absorption spectrum at the corners. (i) Spatial intensity profiles showing localized corner modes.

quadrupole moment, which contributes to the robustness of corner states against disorder. The system in Fig. 4(f) has four corner states in the bandgap. The energy spectrum and absorption spectrum of the corner states are shown in Figs. 4(g) and 4(h), respectively. The corner states show a highly localized spatial intensity profile in Fig. 4(i). In contrast, corner states in a lattice with no quadruple moment will significantly couple to the bulk modes. Based on couple cavities, the research of higher-order states can further extend to non-Hermitian systems, where the corner modes can be localized only at one corner[136,137]. Quadruple photonic crystals without dipole polarization can be achieved using gyromagnetic materials[138]. Future studies may be carried out in 3D topological photonics to realize topological hinge states and corner states[139–141].

Highly localized topological corner states have inspired the design of high-Q devices[142]. For example, a low-threshold topological nano-laser with a high spontaneous emission coupling factor has been developed based on second-order corner states[143]. The topological nature can also trap information at the corners, which may inspire the design of photonic devices for information storage and processing[144].

6. Conclusion

Topological-protected wave manipulation has numerous novel applications and can result in robust optical devices, which indicates a bright future for real applications in topological photonics. The most straightforward applications exploit the topologically protected unidirectional edge states as robust optical delay lines or isolators. The topological phenomenon can be used in the development of lasers, amplifiers, and light sources to improve their performance. The robust transport of photons also boosts the development of photonic topological quantum information processing and quantum computing. Although the practical application of topological photonic devices is still a challenge, especially in the optical frequency regime, topological photonics has greatly advanced fundamental physics and light technology.

Acknowledgement

This work was supported by the National Key Research and Development Program of China (Nos. 2016YFA0301102 and 2017YFA0303800), the National Natural Science Fund for Distinguished Young Scholars (No. 11925403), the National Natural Science Foundation of China (Nos. 11974193, 91856101, and 11774186), and the Natural Science Foundation of Tianjin for Distinguished Young Scientists (No. 18JCJQJC45700).

References

1. R. A. Shelby, D. R. Smith, and S. Schultz, "Experimental verification of a negative index of refraction," Science **292**, 77 (2001).
2. D. R. Smith, J. B. Pendry, and M. C. K. Wiltshire, "Metamaterials and negative refractive index," Science **305**, 788 (2004).
3. J. B. Pendry, D. Schurig, and D. R. Smith, "Controlling electromagnetic fields," Science **312**, 1780 (2006).
4. A. V. Rogacheva, V. A. Fedotov, A. S. Schwanecke, and N. I. Zheludev, "Giant gyrotropy due to electromagnetic-field coupling in a bilayered chiral structure," Phys. Rev. Lett. **97**, 177401 (2006).
5. S. Chen, Z. Li, Y. Zhang, H. Cheng, and J. Tian, "Phase manipulation of electromagnetic waves with metasurfaces and its applications in nanophotonics," Adv. Opt. Mater. **6**, 1800104 (2018).
6. H. Cheng, Z. Liu, S. Chen, and J. Tian, "Emergent functionality and controllability in few-layer metasurfaces," Adv. Mater. **27**, 5410 (2015).
7. S. Chen, Z. Li, W. Liu, H. Cheng, and J. Tian, "From single-dimensional to multidimensional manipulation of optical waves with metasurfaces," Adv. Mater. **31**, 1802458 (2019).
8. S. Chen, W. Liu, Z. Li, H. Cheng, and J. Tian, "Metasurface-empowered optical multiplexing and multifunction," Adv. Mater. **32**, 1805912 (2020).
9. P. Yu, J. Li, C. Tang, H. Cheng, Z. Liu, Z. Li, Z. Liu, C. Gu, J. Li, S. Chen, and J. Tian, "Controllable optical activity with non-chiral plasmonic metasurfaces," Light Sci. Appl. **5**, e16096 (2016).
10. Z. Liu, Z. Li, Z. Liu, J. Li, H. Cheng, P. Yu, W. Liu, C. Tang, C. Gu, J. Li, S. Chen, and J. Tian, "High-performance broadband circularly polarized beam deflector by mirror effect of multinanorod metasurfaces," Adv. Funct. Mater. **25**, 5428 (2015).
11. Y. Zhang, W. Liu, Z. Li, Z. Li, H. Cheng, S. Chen, and J. Tian, "High-quality-factor multiple Fano resonances for refractive index sensing," Opt. Lett. **43**, 1842 (2018).
12. W. Liu, Z. Li, H. Cheng, C. Tang, J. Li, S. Zhang, S. Chen, and J. Tian, "Metasurface enabled wide-angle Fourier lens," Adv. Mater. **30**, 1706368 (2018).
13. B. Yang, W. Liu, Z. Li, H. Cheng, D.-Y. Choi, S. Chen, and J. Tian, "Ultrahighly saturated structural colors enhanced by multipolar-modulated metasurfaces," Nano Lett. **19**, 4221 (2019).
14. G. Li, S. Zhang, and T. Zentgraf, "Nonlinear photonic metasurfaces," Nat. Rev. Mater. **2**, 17010 (2017).
15. Z. Li, W. Liu, Z. Li, C. Tang, H. Cheng, J. Li, X. Chen, S. Chen, and J. Tian, "Tripling the capacity of optical vortices by nonlinear metasurface," Laser Photon. Rev. **12**, 1800164 (2018).
16. E. Yablonovitch, "Inhibited spontaneous emission in solid-state physics and electronics," Phys. Rev. Lett. **58**, 2059 (1987).
17. S. John, "Strong localization of photons in certain disordered dielectric superlattices," Phys. Rev. Lett. **58**, 2486 (1987).
18. J. Li, L. Zhou, C. T. Chan, and P. Sheng, "Photonic band gap from a stack of positive and negative index materials," Phys. Rev. Lett. **90**, 083901 (2003).
19. J. Zhu, J. Christensen, J. Jung, L. Martin-Moreno, X. Yin, L. Fok, X. Zhang, and F. J. Garcia-Vidal, "A holey-structured metamaterial for acoustic deep-subwavelength imaging," Nat. Phys. **7**, 52 (2010).
20. O. Vanbesien and N. Fabre, "Photonic crystal based subwavelength imaging and cloaking optical devices," PIERS Online **5**, 216 (2009).
21. X. Huang, Y. Lai, Z. H. Hang, H. Zheng, and C. T. Chan, "Dirac cones induced by accidental degeneracy in photonic crystals and zero-refractive-index materials," Nat. Mater. **10**, 582 (2011).
22. X. Zhang, "Observing Zitterbewegung for photons near the Dirac point of a two-dimensional photonic crystal," Phys. Rev. Lett. **100**, 113903 (2008).
23. P. Soltan-Panahi, J. Struck, P. Hauke, A. Bick, W. Plenkers, G. Meineke, C. Becker, P. Windpassinger, M. Lewenstein, and K. Sengstock, "Multi-component quantum gases in spin-dependent hexagonal lattices," Nat. Phys. **7**, 434 (2011).
24. K. V. Klitzing, G. Dorda, and M. Pepper, "New method for high-accuracy determination of the fine-structure constant based on quantized hall resistance," Phys. Rev. Lett. **45**, 494 (1980).
25. D. J. Thouless, M. Kohmoto, M. P. Nightingale, and M. den Nijs, "Quantized hall conductance in a two-dimensional periodic potential," Phys. Rev. Lett. **49**, 405 (1982).
26. F. D. M. Haldane and S. Raghu, "Possible realization of directional optical waveguides in photonic crystals with broken time-reversal symmetry," Phys. Rev. Lett. **100**, 013904 (2008).
27. S. Raghu and F. D. M. Haldane, "Analogs of quantum-Hall-effect edge states in photonic crystals," Phys. Rev. A **78**, 33834 (2008).

28. Y. Hatsugai, "Edge states in the integer quantum Hall effect and the Riemann surface of the Bloch function," Phys. Rev. B **48**, 11851 (1993).
29. Y. Hatsugai, "Chern number and edge states in the integer quantum Hall effect," Phys. Rev. Lett. **71**, 3697 (1993).
30. X.-L. Qi, Y.-S. Wu, and S.-C. Zhang, "General theorem relating the bulk topological number to edge states in two-dimensional insulators," Phys. Rev. B **74**, 045125 (2006).
31. S. Liu, W. Lu, Z. Lin, and S. T. Chui, "Magnetically controllable unidirectional electromagnetic waveguiding devices designed with metamaterials," Appl. Phys. Lett. **97**, 201113 (2010).
32. C. He, X.-L. Chen, M.-H. Lu, X.-F. Li, W.-W. Wan, X.-S. Qian, R.-C. Yin, and Y.-F. Chen, "Left-handed and right-handed one-way edge modes in a gyromagnetic photonic crystal," J. Appl. Phys. **107**, 123117 (2010).
33. W. Qiu, Z. Wang, and M. Soljačić, "Broadband circulators based on directional coupling of one-way waveguides," Opt. Express **19**, 22248 (2011).
34. Z. Wang, L. Shen, Z. Yu, X. Zhang, and X. Zheng, "Highly efficient photonic-crystal splitters based on one-way waveguiding," J. Opt. Soc. Am. B **30**, 173 (2013).
35. B. Bahari, R. Tellez-Limon, and B. Kanté, "Topological terahertz circuits using semiconductors," Appl. Phys. Lett. **109**, 143501 (2016).
36. Y. Wu, C. Li, X. Hu, Y. Ao, Y. Zhao, and Q. Gong, "Applications of topological photonics in integrated photonic devices," Adv. Opt. Mater. **5**, 1700357 (2017).
37. X. Ni, C. He, X. Sun, X. Liu, M. Lu, L. Feng, and Y. Chen, "Topologically protected one-way edge mode in networks of acoustic resonators with circulating air flow," New J. Phys. **17**, 053016 (2015).
38. Y. Ding, Y. Peng, Y. Zhu, X. Fan, J. Yang, B. Liang, X. Zhu, X. Wan, and J. Cheng, "Experimental demonstration of acoustic Chern insulators," Phys. Rev. Lett. **122**, 014302 (2019).
39. G. B. Jo, J. Guzman, C. K. Thomas, P. Hosur, A. Vishwanath, and D. M. Stamper-Kurn, "Ultracold atoms in a tunable optical kagome lattice," Phys. Rev. Lett. **108**, 045305 (2012).
40. S. Nakajima, T. Tomita, S. Taie, T. Ichinose, H. Ozawa, L. Wang, M. Troyer, and Y. Takahashi, "Topological Thouless pumping of ultracold fermions," Nat. Phys. **12**, 296 (2016).
41. S. D. Huber, "Topological mechanics," Nat. Phys. **12**, 621 (2016).
42. P. Wang, L. Lu, and K. Bertoldi, "Topological phononic crystals with one-way elastic edge waves," Phys. Rev. Lett. **115**, 104302 (2015).
43. R. Süsstrunk and S. D. Huber, "Observation of phononic helical edge states in a mechanical topological insulator," Science **349**, 6243 (2015).
44. C. L. Kane and E. J. Mele, "Z2 topological order and the quantum spin Hall effect," Phys. Rev. Lett. **95**, 146802 (2005).
45. C. L. Kane and E. J. Mele, "Quantum spin Hall effect in graphene," Phys. Rev. Lett. **95**, 226801 (2005).
46. B. A. Bernevig, T. L. Hughes, and S. C. Zhang, "Quantum spin Hall effect and topological phase transition in HgTe quantum wells," Science **314**, 1757 (2006).
47. M. Konig, S. Wiedmann, C. Brune, A. Roth, H. Buhmann, L. W. Molenkamp, X.-L. Qi, and S.-C. Zhang, "Quantum spin Hall insulator state in HgTe quantum wells," Science **318**, 766 (2007).
48. M. Hafezi, E. A. Demler, M. D. Lukin, and J. M. Taylor, "Robust optical delay lines with topological protection," Nat. Phys. **7**, 907 (2011).
49. M. Hafezi, S. Mittal, J. Fan, A. Migdall, and J. M. Taylor, "Imaging topological edge states in silicon photonics," Nat. Photon. **7**, 1001 (2013).
50. A. P. Slobozhanyuk, A. B. Khanikaev, D. S. Filonov, D. A. Smirnova, A. E. Miroshnichenko, and Y. S. Kivshar, "Experimental demonstration of topological effects in bianisotropic metamaterials," Sci. Rep. **6**, 22270 (2016).
51. A. B. Khanikaev, S. Hossein Mousavi, W.-K. Tse, M. Kargarian, A. H. MacDonald, and G. Shvets, "Photonic topological insulators," Nat. Mater. **12**, 233 (2013).
52. C. He, X.-C. Sun, X.-P. Liu, M.-H. Lu, Y. Chen, L. Feng, and Y.-F. Chen, "Photonic topological insulator with broken time-reversal symmetry," Proc. Natl. Acad. Sci. USA **113**, 4924 (2016).
53. W. J. Chen, S. J. Jiang, X. D. Chen, B. Zhu, L. Zhou, J. W. Dong, and C. T. Chan, "Experimental realization of photonic topological insulator in a uniaxial metacrystal waveguide," Nat. Commun. **5**, 5782 (2014).
54. X. Zhang, M. Xiao, Y. Cheng, M.-H. Lu, and J. Christensen, "Topological sound," Commun. Phys. **1**, 97 (2018).
55. Z. Yang, F. Gao, X. Shi, X. Lin, Z. Gao, Y. Chong, and B. Zhang, "Topological acoustics," Phys. Rev. Lett. **114**, 114301 (2015).
56. C. He, X. Ni, H. Ge, X.-C. Sun, Y.-B. Chen, M.-H. Lu, X.-P. Liu, and Y.-F. Chen, "Acoustic topological insulator and robust one-way sound transport," Nat. Phys. **12**, 1124 (2016).
57. M. Xiao, W.-J. Chen, W.-Y. He, and C. T. Chan, "Synthetic gauge flux and Weyl points in acoustic systems," Nat. Phys. **11**, 920 (2015).
58. B. Xie, H. Liu, H. Cheng, Z. Liu, S. Chen, and J. Tian, "Experimental realization of type-II Weyl points and Fermi arcs in phononic crystal," Phys. Rev. Lett. **122**, 104302 (2019).
59. B. Xie, H. Liu, H. Cheng, Z. Liu, S. Chen, and J. Tian, "Acoustic topological transport and refraction in a Kekulé lattice," Phys. Rev. Appl. **11**, 044086 (2019).
60. B. Yan and C. Felser, "Topological materials: Weyl semimetals," Annu. Rev. Condens. Matter Phys. **8**, 337 (2017).
61. M. S. Rudner, N. H. Lindner, E. Berg, and M. Levin, "Anomalous edge states and the bulk-edge correspondence for periodically driven two-dimensional systems," Phys. Rev. X **3**, 031005 (2013).
62. K. Fang, Z. Yu, and S. Fan, "Realizing effective magnetic field for photons by controlling the phase of dynamic modulation," Nat. Photon. **6**, 782 (2012).
63. S. Mukherjee, A. Spracklen, M. Valiente, E. Andersson, P. Öhberg, N. Goldman, and R. R. Thomson, "Experimental observation of anomalous topological edge modes in a slowly driven photonic lattice," Nat. Commun. **8**, 13918 (2017).
64. L. J. Maczewsky, J. M. Zeuner, S. Nolte, and A. Szameit, "Observation of photonic anomalous Floquet topological insulators," Nat. Commun. **8**, 13756 (2017).
65. O. Zilberberg, S. Huang, J. Guglielmon, M. Wang, K. P. Chen, Y. E. Kraus, and M. C. Rechtsman, "Photonic topological boundary pumping as a probe of 4D quantum Hall physics," Nature **553**, 59 (2018).
66. M. Verbin, O. Zilberberg, Y. Lahini, Y. E. Kraus, and Y. Silberberg, "Topological pumping over a photonic Fibonacci quasicrystal," Phys. Rev. B **91**, 064201 (2015).
67. Y. Ke, X. Qin, F. Mei, H. Zhong, Y. S. Kivshar, and C. Lee, "Topological phase transitions and Thouless pumping of light in photonic waveguide arrays," Laser Photon. Rev. **10**, 995 (2016).
68. H. Zhao, X. Qiao, T. Wu, B. Midya, S. Longhi, and L. Feng, "Non-Hermitian topological light steering," Science **365**, 1163 (2019).
69. B. Zhen, C. W. Hsu, Y. Igarashi, L. Lu, I. Kaminer, A. Pick, S.-L. Chua, J. D. Joannopoulos, and M. Soljačić, "Spawning rings of exceptional points out of Dirac cones," Nature **525**, 354 (2015).
70. T. E. Lee, "Anomalous edge state in a non-Hermitian lattice," Phys. Rev. Lett. **116**, 133903 (2016).
71. A. Regensburger, C. Bersch, M. A. Miri, G. Onishchukov, D. N. Christodoulides, and U. Peschel, "Parity-time synthetic photonic lattices," Nature **488**, 167 (2012).
72. H. Hodaei, M.-A. Miri, M. Heinrich, D. N. Christodoulides, and M. Khajavikhan, "Parity-time-symmetric microring lasers," Science **346**, 975 (2014).
73. S. Longhi, "PT-symmetric laser absorber," Phys. Rev. A **82**, 031801 (2010).
74. Y. D. Chong, L. Ge, and A. D. Stone, "PT-symmetry breaking and laser-absorber modes in optical scattering systems," Phys. Rev. Lett. **106**, 093902 (2011).
75. L. Feng, Y. L. Xu, W. S. Fegadolli, M. H. Lu, J. E. B. Oliveira, V. R. Almeida, Y. F. Chen, and A. Scherer, "Experimental demonstration of a unidirectional reflectionless parity-time metamaterial at optical frequencies," Nat. Mater. **12**, 108 (2013).
76. L. Feng, Z. J. Wong, R. M. Ma, Y. Wang, and X. Zhang, "Single-mode laser by parity-time symmetry breaking," Science **346**, 972 (2014).
77. D. Leykam and Y. D. Chong, "Edge solitons in nonlinear-photonic topological insulators," Phys. Rev. Lett. **117**, 143901 (2016).
78. A. N. Poddubny and D. A. Smirnova, "Ring Dirac solitons in nonlinear topological systems," Phys. Rev. A **98**, 013827 (2018).
79. Y. Hadad, A. B. Khanikaev, and A. Alù, "Self-induced topological transitions and edge states supported by nonlinear staggered potentials," Phys. Rev. B **93**, 155112 (2016).
80. Y. Lumer, Y. Plotnik, M. C. Rechtsman, and M. Segev, "Self-localized states in photonic topological insulators," Phys. Rev. Lett. **111**, 243905 (2013).
81. A. D. Greentree, C. Tahan, J. H. Cole, and L. C. L. Hollenberg, "Quantum phase transitions of light," Nat. Phys. **2**, 856 (2006).
82. M. J. Hartmann, F. G. S. L. Brando, and M. B. Plenio, "Strongly interacting polaritons in coupled arrays of cavities," Nat. Phys. **2**, 849 (2006).

83. D. G. Angelakis, M. F. Santos, and S. Bose, "Photon-blockade-induced Mott transitions and *XY* spin models in coupled cavity arrays," Phys. Rev. A **76**, 031805 (2007).
84. S. Tsesses, E. Ostrovsky, K. Cohen, B. Gjonaj, N. H. Lindner, and G. Bartal, "Optical skyrmion lattice in evanescent electromagnetic fields," Science **361**, 993 (2018).
85. L. Du, A. Yang, A. V. Zayats, and X. Yuan, "Deep-subwavelength features of photonic skyrmions in a confined electromagnetic field with orbital angular momentum," Nat. Phys. **15**, 650 (2019).
86. Z. Wang, Y. D. Chong, J. D. Joannopoulos, and M. Soljačić, "Reflection-free one-way edge modes in a gyromagnetic photonic crystal," Phys. Rev. Lett. **100**, 013905 (2008).
87. Z. Wang, Y. Chong, J. D. Joannopoulos, and M. Soljačić, "Observation of unidirectional backscattering-immune topological electromagnetic states," Nature **461**, 772 (2009).
88. S. A. Skirlo, L. Lu, Y. Igarashi, Q. Yan, J. Joannopoulos, and M. Soljačić, "Experimental observation of large Chern numbers in photonic crystals," Phys. Rev. Lett. **115**, 253901 (2015).
89. S. A. Skirlo, L. Lu, and M. Soljačić, "Multimode one-way waveguides of large Chern numbers," Phys. Rev. Lett. **113**, 113904 (2014).
90. L. Lu, H. Gao, and Z. Wang, "Topological one-way fiber of second Chern number," Nat. Commun. **9**, 5384 (2018).
91. K. Liu, L. Shen, and S. He, "One-way edge mode in a gyromagnetic photonic crystal slab," Opt. Lett. **37**, 4110 (2012).
92. C. He, X.-L. Chen, M.-H. Lu, X.-F. Li, W.-W. Wan, X.-S. Qian, R.-C. Yin, and Y.-F. Chen, "Tunable one-way cross-waveguide splitter based on gyromagnetic photonic crystal," Appl. Phys. Lett. **96**, 111111 (2010).
93. C. Huang and C. Jiang, "Nonreciprocal photonic crystal delay waveguide," J. Opt. Soc. Am. B **26**, 1954 (2009).
94. X. Zang and C. Jiang, "Edge mode in nonreciprocal photonic crystal waveguide: manipulating the unidirectional electromagnetic pulse dynamically," J. Opt. Soc. Am. B **28**, 554 (2011).
95. L.-H. Wu and X. Hu, "Scheme for achieving a topological photonic crystal by using dielectric material," Phys. Rev. Lett. **114**, 223901 (2015).
96. Y. Yang, Y. F. Xu, T. Xu, H. X. Wang, J. H. Jiang, X. Hu, and Z. H. Hang, "Visualization of a unidirectional electromagnetic waveguide using topological photonic crystals made of dielectric materials," Phys. Rev. Lett. **120**, 217401 (2018).
97. T. Ma and G. Shvets, "All-Si valley-Hall photonic topological insulator," New J. Phys. **18**, 025012 (2016).
98. J.-W. Dong, X.-D. Chen, H. Zhu, Y. Wang, and X. Zhang, "Valley photonic crystals for control of spin and topology," Nat. Mater. **16**, 298 (2017).
99. S. Yves, R. Fleury, F. Lemoult, M. Fink, and G. Lerosey, "Topological acoustic polaritons: robust sound manipulation at the subwavelength scale," New J. Phys. **19**, 075003 (2017).
100. M. A. Gorlach, X. Ni, D. A. Smirnova, D. Korobkin, D. Zhirihin, A. P. Slobozhanyuk, P. A. Belov, A. Alù, and A. B. Khanikaev, "Far-field probing of leaky topological states in all-dielectric metasurfaces," Nat. Commun. **9**, 909 (2018).
101. S. Barik, A. Karasahin, C. Flower, T. Cai, H. Miyake, W. DeGottardi, M. Hafezi, and E. Waks, "A topological quantum optics interface," Science **359**, 666 (2018).
102. A. Slobozhanyuk, S. H. Mousavi, X. Ni, D. Smirnova, Y. S. Kivshar, and A. B. Khanikaev, "Three-dimensional all-dielectric photonic topological insulator," Nat. Photonics **11**, 130 (2017).
103. Y. Yang, Z. Gao, H. Xue, L. Zhang, M. He, Z. Yang, R. Singh, Y. Chong, B. Zhang, and H. Chen, "Realization of a three-dimensional photonic topological insulator," Nature **565**, 622 (2019).
104. L. Lu, C. Fang, L. Fu, S. G. Johnson, J. D. Joannopoulos, and M. Soljačić, "Symmetry-protected topological photonic crystal in three dimensions," Nat. Phys. **12**, 337 (2016).
105. A. Burkov, "Topological semimetals," Nat. Mater. **15**, 1145 (2016).
106. J. Xiong, S. K. Kushwaha, T. Liang, J. W. Krizan, M. Hirschberger, W. Wang, R. J. Cava, and N. P. Ong, "Evidence for the chiral anomaly in the Dirac semimetal Na_3Bi," Science **350**, 413 (2015).
107. A. C. Potter, I. Kimchi, and A. Vishwanath, "Quantum oscillations from surface Fermi arcs in Weyl and Dirac semimetals," Nat. Commun. **5**, 5161 (2014).
108. X. Wan, A. M. Turner, A. Vishwanath, and S. Y. Savrasov, "Topological semimetal and Fermi-arc surface states in the electronic structure of pyrochlore iridates," Phys. Rev. B **83**, 205101 (2011).
109. S. M. Young, S. Zaheer, J. C. Y. Teo, C. L. Kane, E. J. Mele, and A. M. Rappe, "Dirac semimetal in three dimensions," Phys. Rev. Lett. **108**, 140405 (2012).
110. A. A. Burkov, M. D. Hook, and L. Balents, "Topological nodal semimetals," Phys. Rev. B **84**, 235126 (2011).
111. M. Xiao, Q. Lin, and S. Fan, "Hyperbolic Weyl point in reciprocal chiral metamaterials," Phys. Rev. Lett. **117**, 057401 (2016).
112. L. Lu, L. Fu, J. D. Joannopoulos, and M. Soljačić, "Weyl points and line nodes in gyroid photonic crystals," Nat. Photon. **7**, 294 (2013).
113. H. Cheng, W. Gao, Y. Bi, W. Liu, Z. Li, Q. Guo, Y. Yang, O. You, J. Feng, H. Sun, J. Tian, S. Chen, and S. Zhang, "Vortical reflection and spiraling Fermi arcs with Weyl metamaterials," Phys. Rev. Lett. **125**, 093904 (2020).
114. W. Gao, B. Yang, M. Lawrence, F. Fang, B. Béri, and S. Zhang, "Photonic Weyl degeneracies in magnetized plasma," Nat. Commun. **7**, 12435 (2016).
115. J. Bravo-Abad, L. Lu, L. Fu, H. Buljan, and M. Soljačić, "Weyl points in photonic-crystal superlattices," 2D Mater. **2**, 034013 (2015).
116. C. Liu, W. Gao, B. Yang, and S. Zhang, "Disorder-induced topological state transition in photonic metamaterials," Phys. Rev. Lett. **119**, 183901 (2017).
117. W. Gao, M. Lawrence, B. Yang, F. Liu, F. Fang, B. Béri, J. Li, and S. Zhang, "Topological photonic phase in chiral hyperbolic metamaterials," Phys. Rev. Lett. **114**, 037402 (2015).
118. J. Noh, S. Huang, D. Leykam, Y. D. Chong, K. P. Chen, and M. C. Rechtsman, "Experimental observation of optical Weyl points and Fermi arc-like surface states," Nat. Phys. **13**, 611 (2017).
119. M. Trescher, B. Sbierski, P. W. Brouwer, and E. J. Bergholtz, "Quantum transport in Dirac materials: signatures of tilted and anisotropic Dirac and Weyl cones," Phys. Rev. B **91**, 115135 (2015).
120. Q. Guo, B. Yang, L. Xia, W. Gao, H. Liu, J. Chen, Y. Xiang, and S. Zhang, "Three dimensional photonic Dirac points in metamaterials," Phys. Rev. Lett. **119**, 213901 (2017).
121. Q. Guo, O. You, B. Yang, J. B. Sellman, E. Blythe, H. Liu, Y. Xiang, J. Li, D. Fan, J. Chen, C. T. Chan, and S. Zhang, "Observation of three-dimensional photonic Dirac points and spin-polarized surface arcs," Phys. Rev. Lett. **122**, 203903 (2019).
122. W. Deng, J. Lu, F. Li, X. Huang, M. Yan, J. Ma, and Z. Liu, "Nodal rings and drumhead surface states in phononic crystals," Nat. Commun. **10**, 1769 (2019).
123. T. Kawakami and X. Hu, "Symmetry-guaranteed nodal-line semimetals in an FCC lattice," Phys. Rev. B **96**, 235307 (2017).
124. Q. Yan, R. Liu, Z. Yan, B. Liu, H. Chen, Z. Wang, and L. Lu, "Experimental discovery of nodal chains," Nat. Phys. **14**, 461 (2018).
125. Z. Yan, R. Bi, H. Shen, L. Lu, S.-C. Zhang, and Z. Wang, "Nodal-link semimetals," Phys. Rev. B **96**, 041103 (2017).
126. W. A. Benalcazar, B. A. Bernevig, and T. L. Hughes, "Quantized electric multipole insulators," Science **357**, 61 (2017).
127. C. W. Peterson, W. A. Benalcazar, T. L. Hughes, and G. Bahl, "A quantized microwave quadrupole insulator with topologically protected corner states," Nature **555**, 346 (2018).
128. M. Serra-Garcia, V. Peri, R. Süsstrunk, O. R. Bilal, T. Larsen, L. G. Villanueva, and S. D. Huber, "Observation of a phononic quadrupole topological insulator," Nature **555**, 342 (2018).
129. H. Xue, Y. Yang, F. Gao, Y. Chong, and B. Zhang, "Acoustic higher-order topological insulator on a kagome lattice," Nat. Mater. **18**, 108 (2019).
130. M. Li, D. Zhirihin, M. Gorlach, X. Ni, D. Filonov, A. Slobozhanyuk, A. Alù, and A. B. Khanikaev, "Higher-order topological states in photonic kagome crystals with long-range interactions," Nat. Photon. **14**, 89 (2020).
131. A. El Hassan, F. K. Kunst, A. Moritz, G. Andler, E. J. Bergholtz, and M. Bourennane, "Corner states of light in photonic waveguides," Nat. Photon. **13**, 697 (2019).
132. B.-Y. Xie, H.-F. Wang, H.-X. Wang, X.-Y. Zhu, J.-H. Jiang, M.-H. Lu, and Y.-F. Chen, "Second-order photonic topological insulator with corner states," Phys. Rev. B **98**, 205147 (2018).
133. B. Y. Xie, G. X. Su, H. F. Wang, H. Su, X. P. Shen, P. Zhan, M. H. Lu, Z. L. Wang, and Y. F. Chen, "Visualization of higher-order topological insulating phases in two-dimensional dielectric photonic crystals," Phys. Rev. Lett. **122**, 233903 (2019).

134. X. D. Chen, W. M. Deng, F. L. Shi, F. L. Zhao, M. Chen, and J. W. Dong, "Direct observation of corner states in second-order topological photonic crystal slabs," Phys. Rev. Lett. **122**, 233902 (2019).
135. S. Mittal, V. V. Orre, G. Zhu, M. A. Gorlach, A. Poddubny, and M. Hafezi, "Photonic quadrupole topological phases," Nat. Photon. **13**, 692 (2019).
136. X.-W. Luo and C. Zhang, "Higher-order topological corner states induced by gain and loss," Phys. Rev. Lett. **123**, 073601 (2019).
137. T. Liu, Y.-R. Zhang, Q. Ai, Z. Gong, K. Kawabata, M. Ueda, and F. Nori, "Second-order topological phases in non-Hermitian systems," Phys. Rev. Lett. **122**, 076801 (2019).
138. L. He, Z. Addison, E. J. Mele, and B. Zhen, "Quadrupole topological photonic crystals," Nat. Commun. **11**, 3119 (2020).
139. F. Schindler, A. M. Cook, M. G. Vergniory, Z. Wang, S. S. P. Parkin, B. A. Bernevig, and T. Neupert, "Higher-order topological insulators," Sci. Adv. **4**, eaat0346 (2018).
140. O. Pozo, C. Repellin, and A. G. Grushin, "Quantization in chiral higher order topological insulators: circular dichroism and local Chern marker," Phys. Rev. Lett. **123**, 247401 (2019).
141. Z. Song, Z. Fang, and C. Fang, "(d−2)-dimensional edge states of rotation symmetry protected topological states," Phys. Rev. Lett. **119**, 246402 (2017).
142. X. Xie, W. Zhang, X. He, S. Wu, J. Dang, K. Peng, F. Song, L. Yang, H. Ni, Z. Niu, C. Wang, K. Jin, X. Zhang, and X. Xu, "Cavity quantum electrodynamics with second-order topological corner state," Laser Photon. Rev. **14**, 1900425 (2020).
143. W. Zhang, X. Xie, H. Hao, J. Dang, S. Xiao, S. Shi, H. Ni, Z. Niu, C. Wang, K. Jin, X. Zhang, and X. Xu, "Low-threshold topological nanolasers based on the second-order corner state," Light Sci. Appl. **9**, 109 (2020).
144. R. Banerjee, S. Mandal, and T. C. H. Liew, "Coupling between exciton-polariton corner modes through edge states," Phys. Rev. Lett. **124**, 063901 (2020).

221.238.245.28 [2021-08-31 09:48:57]